BUTTERWORTH HEINEMANN

Polymer Vol. 36 No. 21, pp. 4039–4054, 1995
Elsevier Science Ltd
Printed in Great Britain

Molecular mechanism of neck formation in uniaxially stretched poly(ethylene naphthalate) films

M. Cakmak* and S. W. Lee
Polymer Engineering Institute, College of Polymer Engineering and Polymer Science, University of Akron, Akron, OH 44325-0301, USA
(Received 6 January 1995; revised 1 May 1995)

When amorphous poly(ethylene-2,6-naphthalate) (PEN) sheets are stretched between the glass transition temperature and the cold crystallization temperature, they exhibit necking. The occurrence of this unusual neck formation above the glass transition temperature causes large local fluctuations in the thickness of samples. However, uniformity of sample thickness can be re-established when the films are stretched beyond the critical strain at which stress hardening due to crystallization starts to occur. To elucidate the mechanism of neck formation in films stretched up to 20–30°C above the glass transition temperature, a series of samples were prepared under selected conditions and were sliced in the machine direction–normal direction (MD–ND) plane. The structural variations along the necked region were analysed using optical retardation, infra-red dichroism and micro-beam X-ray diffraction techniques. The results obtained from these techniques indicate that, during the course of deformation, the naphthalene groups, which are large and highly planar, rapidly align their broad faces parallel to the surface of the flat film. This behaviour resembles a disorder–nematic order transition and occurs at highly localized regions in the sample, thereby manifesting itself macroscopically as a neck. The free-width uniaxially stretched films were found to exhibit uniplanar axial texture instead of the expected transverse isotropy as a result of this preferential orientation of the naphthalene planes.

(Keywords: poly(ethylene naphthalate); uniaxially stretched film; neck formation)

INTRODUCTION

Poly(ethylene-2,6-naphthalate) (PEN) is produced by condensation polymerization of 2,6-naphthalenedicarboxylic acid and ethylene glycol[1–4]. This polymer, like poly(ethylene terephthalate) (PET), can be formed into amorphous form by quenching from the melt or it can be crystallized either by slow cooling from the melt or by stretching between the glass transition temperature and the cold crystallization temperature. It can also be crystallized from the amorphous phase by exposing the polymer to solvents such as dioxane and methylene chloride[4] and aniline[5]. PEN exhibits a glass transition temperature of about 120°C, which makes it quite attractive as a high-temperature polymer for film, tape[6,7] and moulding applications.

There are two known crystal structures of PEN. The first one (called α) was discovered by Mencik[2]. He reported that it is a triclinic unit cell with the unit-cell parameters $a = 0.651$ nm, $b = 0.575$ nm, $c = 1.32$ nm, $\alpha = 81.33°$, $\beta = 144°$ and $\gamma = 100°$. The density is 1.407 g cm^{-3}. The naphthalene planes are nearly parallel to the $(\bar{1}\,1\,0)$ planes, making a 9° angle with this plane. This α form is generally obtained when the polymer is crystallized from the amorphous phase or from the melt below 240°C. When PEN is crystallized above about 240°C, it exhibits a second crystal structure (called β)[8]. This form is also triclinic, with the following unit-cell parameters: $a = 0.926$ nm, $b = 1.559$ nm, $c = 1.273$ nm, $\alpha = 121.6°$, $\beta = 95.57°$, $\gamma = 122.52°$, and density $\rho = 1.439$ g cm^{-3}.

An increase of the melting temperature to a temperature far above 270°C was also observed by annealing at temperatures close to the melting temperature. Buchner *et al.*[8] suggested that high melting temperature is a result of change of crystal surface morphology by transesterification reactions. Wunderlich *et al.*[9] determined the equilibrium melting parameters as $T_m^\circ = 337$°C, $\Delta H_f = 25 \pm 2.0$ kJ mol^{-1} and $\Delta S_f = 41 \pm 3.3$ J K^{-1} mol^{-1}.

There have been several studies on the influence of processing conditions on the structure and properties of PEN. These include solid-state extrusion[10], uniaxial film stretching[11,12] and biaxial film stretching[3]. Extensive research on structure development of uni- and biaxially drawn PEN films has been performed in our group[3]. In this research, we observed that initially amorphous PEN exhibits necking behaviour during drawing even above the glass transition temperature. During stretching with both uni- and biaxial modes, PEN undergoes uniform deformation before necking starts. Then, a neck develops and propagates in the sample up to the onset of stress hardening, and if films are further stretched they become uniform again. Optimum-quality films could be

* To whom correspondence should be addressed

Table 1 Intrinsic viscosities of PEN films

Sample designation	Intrinsic viscosity ($dl\,g^{-1}$)	
	Resin	Film
PEN5	0.63	0.59
PEN6	0.72	0.68

obtained in the 135–155°C range at high stretch ratios with $5\,mm\,s^{-1}$ or higher drawing speeds. The crystal structure of drawn and annealed film was found to be the low-temperature modification (α). In addition, it was found that naphthalene planes were arranged parallel to the film surface in the case of biaxial drawing. Biaxial drawing was found to improve the modulus, yield strength and tensile strength, but reduced the elongation at break. PEN shows much lower creep strains than PET owing to its higher T_g. These creep properties were found to be improved substantially by annealing as a result of increases in crystallinity.

Morphological aspects of necking mechanism

The research that has been done in the past identified three stages in the low-temperature deformation in semicrystalline polymers[13–23]. These are: (i) plastic deformation of the original spherulitic structure; (ii) the discontinuous transformation of the spherulitic into a fibrillar structure by micronecking; and (iii) plastic deformation of the fibrillar structure[24]. When the temperature is increased, the highly localized neck slowly disappears as a result of the distribution of deformation over a large number of sites. This is a result of an increase in molecular mobility, which significantly reduces the yield stress, thereby causing the nucleation of deformation at a large number of sites.

Phenomenological aspects of yield process

Early investigations on thermal effects during deformation suggested that necking developed because of strain softening produced by a local temperature rise[25]. Ward[26] calculated the temperature rise caused by the drawing process on the basis of experimental results, assuming that the yield stress as well as the drawing stress are the forces necessary to initiate large-scale molecular motion and that similar mechanisms are operative in both initial yielding and the subsequent propagation of the neck. The difference between the drawing stress on the assumption of an isothermal process and that measured experimentally was attributed to an increase in sample temperature.

Lazurkin[27] observed cold drawing in elastomers at very low strain rates and noted that necking can still take place under quasi-static conditions. Vincent[28] confirmed this result by showing that cold drawing occurs in polyethylene at very low strain rates at room temperature and concluded that cold drawing is caused by mechanical instability followed by a strain-hardening process, due to molecular orientation.

Although necking has been observed in polycarbonate and similar materials, we have not found a molecular explanation for necking in amorphous polymers. The observation of this anomalous necking behaviour in essentially amorphous PEN films above their glass transition temperature prompted the present investigation as to its molecular mechanism.

EXPERIMENTAL

Materials

PEN films of 0.7 mm thickness were provided by Goodyear Tire and Rubber Co. These films were cast using a 6.4 cm Egan Extruder equipped with a 75 cm die and a three-roll stand. The intrinsic viscosities were determined by dissolving the polymers in a mixture of phenol/tetrachloroethane/*p*-chlorophenol (25/35/40 wt%) at 140°C. These data, furnished by Goodyear Tire and Rubber Co., are given in *Table 1*. In processing of the samples, the temperature in the last zone of the extruder was set at 305°C and the die temperature was set to 277°C. The chill roll temperature was maintained at 52°C.

Thermal characterization

Thermal characterization of amorphous PEN was carried out by using a DuPont 9900 thermal analyser. Before each run the d.s.c. cell was calibrated with an indium standard. The PEN films (about 10 mg) were punched into circular pieces and placed and crimped in aluminium d.s.c. pans. All the scans were performed at $5°C\,min^{-1}$ heating rate in a dry nitrogen atmosphere. Typical d.s.c. scans of as-received sheets were shown in *Figure 1* for both low- (PEN5) and high- (PEN6) molecular-weight polymers. The T_g for these samples are observed around 120°C, the cold crystallization peak temperature around 200°C and the melting temperature at 265°C.

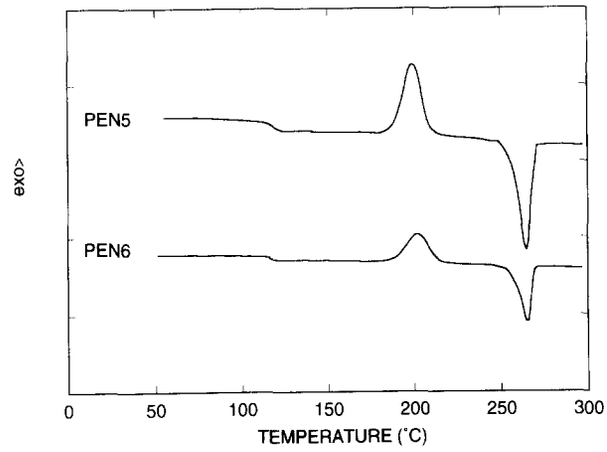

Figure 1 D.s.c. scans for as-cast PEN5 and PEN6

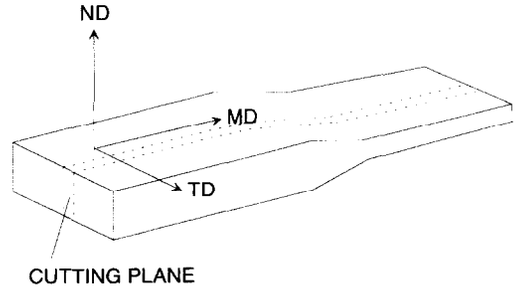

Figure 2 Sample cutting procedure

Uniaxial deformation

Amorphous PEN films were cut into dumbbell shape with a gauge length of 40 mm and a width of 3 mm. Uniaxial deformation of films was carried out at various temperatures and drawing speeds using a Monsanto tensile tester (T10) equipped with a Monsanto convection oven. Before drawing, the sample was equilibrated at the desired temperature for 5 min in the preheated convection oven and drawn to selected draw ratios at selected rates.

To examine the effect of drawing temperature on tensile properties, PEN samples were drawn at 102, 125, 130, 135, 142, 147 and 175°C at a drawing speed of 10 mm s^{-1}. PEN films were drawn at 135°C at various drawing rates ranging from 0.1 to 17 mm s^{-1}. Five samples were drawn at each condition.

Characterization of neck region

Sample preparation. In order to investigate the deformation behaviour, samples of 3 cm × 10 cm were cut from as-received cast sheets. These samples were introduced into the Monsanto convection oven preheated to the desired temperature in the range 103–165°C and after 5 min of temperature equilibration they were stretched to a total strain of 3 ($\epsilon = \Delta l/l_0$) at various extension rates. After the stretching was completed, the samples were cooled to room temperature and removed from the clamps.

To investigate the structural profiles in thickness (normal direction, ND) and along the machine direction (MD), the necked portions of the samples were mounted on a Reichert Histo Stat rotary microtome and thin slices of 30 μm were cut in the MD–ND plane (*Figure 2*).

Birefringence. Birefringence Δn_{13} (1 = MD and 3 = ND) variation along the machine and normal directions through the neck region of the samples were determined using a Leitz Labolux 12 Pol polarized optical microscope equipped with a 30-order Berec compensator.

FT*i.r. spectra.* The i.r. absorption spectra were obtained using a Perkin Elmer 16 pc spectrometer equipped with an i.r. microscope and a wire grid polarizer. Absorption measurements were made at normal incidence along the mid-plane of the neck using 8 cm^{-1} resolution from 4000 to 450 cm^{-1}. Spectra were recorded

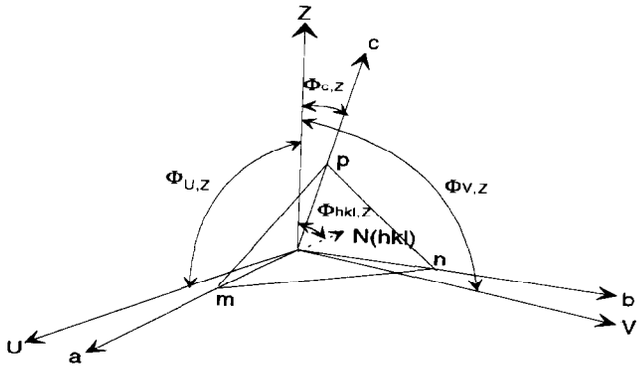

Figure 3 Coordinate system

Table 2 Angle between axes of pseudo-orthorhombic cell and poles of selected planes

	U axis	*V* axis	*c* axis
1 0 0 pole	28.69°	61.31°	90°
$\bar{1}$ 1 0 pole	4.71°	85.29°	90°

for the plane of polarization parallel to the draw direction and normal to the film surface respectively.

Dichroic ratios were obtained from three peaks, 1600 and 1500 cm^{-1} (assigned to naphthalene ring vibration) and 765 cm^{-1} (assigned to naphthalene ring CH out-of-plane bending motion).

Micro-beam X-ray diffraction. The neck region was also characterized using a matrixing micro-beam WAXS camera developed in our laboratories. In this camera, the sample is mounted on a precision *XY* stage and WAXS patterns obtained without removal of the sample from the stage, thus preserving spatial registry between consecutive patterns. This camera was mounted on a Rigaku 12 kW rotating-anode generator, which was operated at 40 kV and 100 mA. The beam from the copper target was monochromatized with a nickel filter and collimated to a diameter of 100 μm. Six WAXS patterns were taken for each drawn sample at 130 μm intervals through the necked region with the beam along the transverse direction (TD). On selected samples WAXS flat-film patterns were taken with the X-ray beam along the normal direction (ND).

Chain-axis and naphthalene-plane normal orientation factor determination

The azimuthal intensity distribution of each wide-angle X-ray diffraction was obtained by digitizing the WAXS patterns using an eight-bit video camera. After a correction for the non-linearity of the X-ray films, $\langle\cos^2\chi\rangle$ values were obtained from the following equation:

$$\langle\cos^2\chi_{hkl,Z}\rangle = \frac{\int_0^{\pi/2} I(\chi)\sin\chi\cos^2\chi\,d\chi}{\int_0^{\pi/2} I(\chi)\sin\chi\,d\chi} \quad (1)$$

To determine the orientation factors for the *c* axes and the physically significant direction normal to the naphthalene planes, we defined a pseudo-orthorhombic unit cell about the PEN single chain. The axes of this unit cell are defined as follows: *U* axis is normal to the ($\bar{4}$ 3 0) plane of the original triclinic cell, which is parallel to the naphthalene planes; *c* axis is along the chain axis; and *V* axis is normal to the *Uc* plane, as shown in *Figure 3*. Angles between the axes of the pseudo-orthorhombic cell and the poles of selected planes in the original triclinic cell are listed in *Table 2*.

The data from $\langle\cos^2\chi_{100,Z}\rangle$ and $\langle\cos^2\chi_{\bar{1}10,Z}\rangle$ were used to determine the $\langle\cos^2\chi_{U,Z}\rangle$ and $\langle\cos^2\chi_{c,Z}\rangle$ values. From Wilchinsky's[29,30] rule the mean-square cosines of *U* and *c* axes become, for *U* axis (normal to naphthalene ring plane):

$$\langle\cos^2\chi_{U,Z}\rangle = \frac{f_2^2\langle\cos^2\chi_{\bar{1}10,Z}\rangle - f_1^2\langle\cos^2\chi_{100,Z}^2\rangle}{e_1^2 f_2^2 - e_2^2 f_1^2} \quad (2)$$

and for c axis:

$$\langle \cos^2 \chi_{c,Z} \rangle = \frac{(e_2^2 - f_2^2)\langle \cos^2 \chi_{100,Z} \rangle - (e_1^2 - f_1^2)\langle \cos^2 \chi_{100,Z} \rangle + e_1^2 f_2^2 - e_2^2 f_1^2}{e_1^2 f_2^2 - e_2^2 f_1^2} \quad (3)$$

Here e, f and g are direction cosines for each plane and $N_{110} = e_1 i + f_1 j + g_1 k$ and $N_{100} = e_2 i + f_2 j + g_2 k$.

RESULTS AND DISCUSSION

Effect of temperature on deformation behaviour

In order to investigate the effect of temperature on the stress–strain behaviour, amorphous PEN5 and PEN6 were stretched both below (102°C) and above ($T > 120$°C) the glass transition temperature. Typical engineering stress–strain curves for PEN5 are presented in *Figure 4*.

Near the glass transition temperature (~ 120°C), three distinct regions on the curves were observed: initially the stress rises in a linear manner, followed by a fall after the yield point; after a period of drawing with relatively constant stress levels, stress starts to rise again as a result of hardening associated with stress-induced crystallization. In this temperature range, necking and cold drawing occur. As the temperature is increased, the region from the yield point (initial maximum) to the minimum drawing stress broadens while the actual yield stress level decreases. This, in turn, causes nucleation of a larger number of necks as a result of greater molecular mobility. These micronecks are distributed uniformly over the sample; thereby whole deformation behaviour approaches quasi-rubber-like deformation (homogeneous). Around 150–170°C the polymers exhibit 'taffy-pull' characteristics without showing

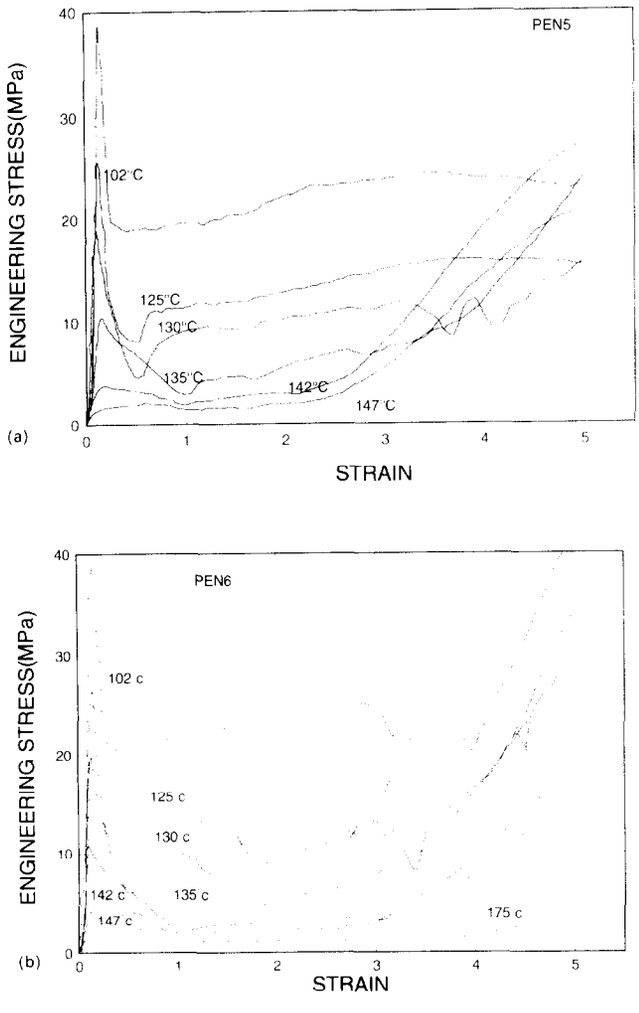

Figure 4 Engineering stress vs. strain for (a) PEN films and (b) PEN6 samples stretched at various temperatures

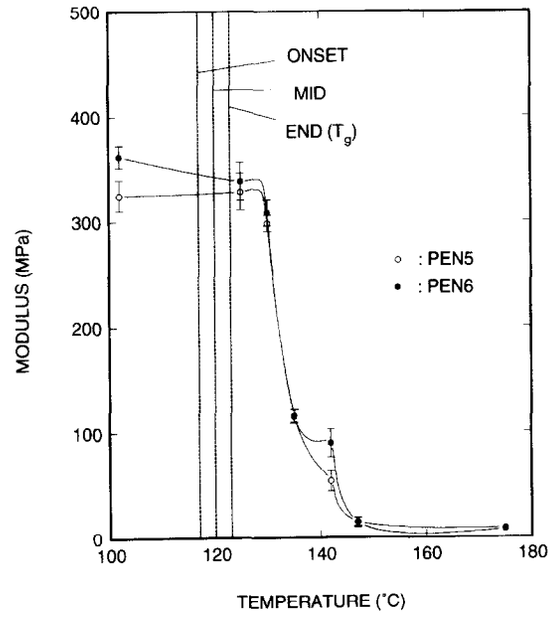

Figure 5 Modulus as a function of temperature for PEN5 and PEN6

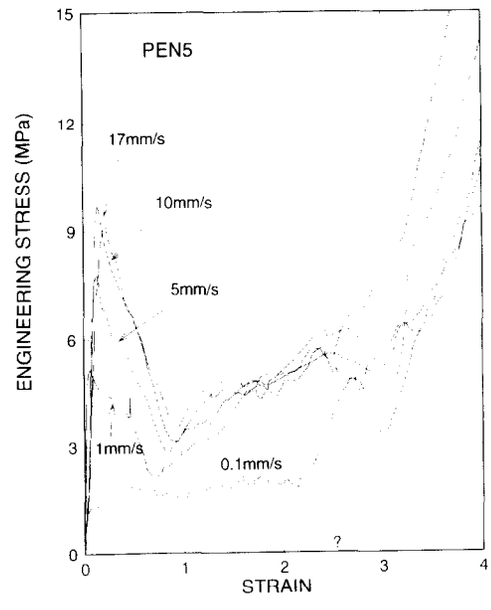

Figure 6 Effect of stretching rate on the stress–strain behaviour of PEN5 (the data for large strains are not shown)

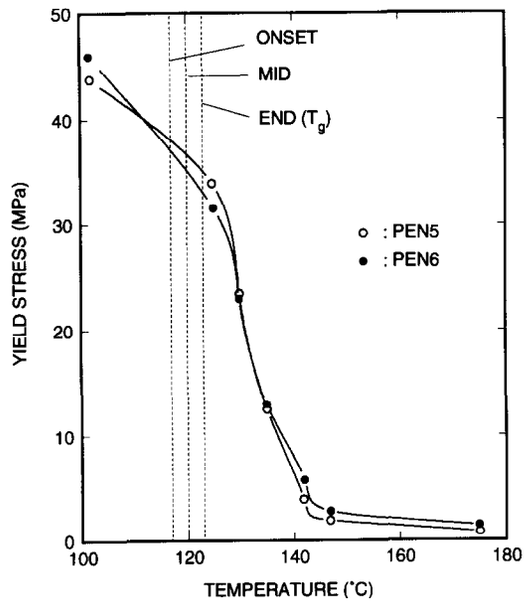

Figure 7 Yield stress as a function of temperature for PEN5 and PEN6

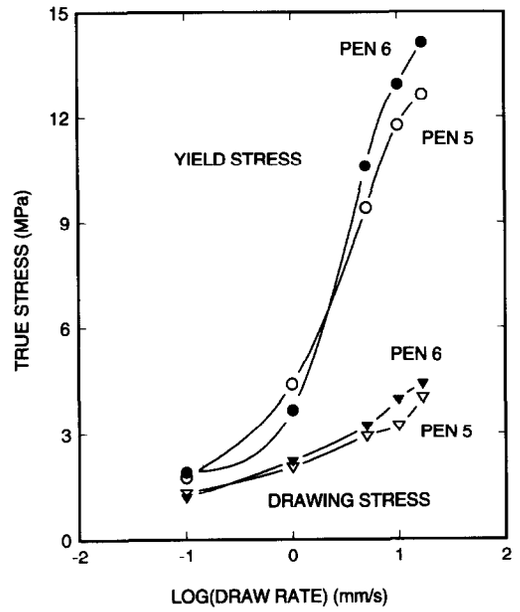

Figure 8 Yield and drawing stresses as a function of draw rate

appreciable strain hardening. The temperature in this range is too high for adequate interchain friction to result in strain hardening and too low for appreciable thermally induced crystallization during the course of deformation.

Figure 5 shows the modulus of samples as a function of temperature. For clarity, the glass transition regions of these samples are indicated with vertical dotted lines in this figure. Modulus decreases through the glass transition region; however, the largest drop occurs about 10°C above T_g and significant modulus values are observed at temperatures up to 145°C. As expected, higher-molecular-weight PEN6 shows slightly higher modulus values.

Draw-rate effect on stress–strain behaviour

Figure 6 shows an enlarged view of the low-strain region of the engineering stress–strain curves on samples stretched at 135°C with drawing rates ranging from 0.1 to 17 mm s^{-1}. At lowest strain rate, no apparent yield stress can be observed and the whole curve resembles that of a vulcanized rubber. As the rate of stretching increases, a clear yield region is observed and the yield stress increases with increase of strain rate. The engineering stress is higher when the drawing rate increases from 0.1 to 17 mm s^{-1}.

Stress hardening is observed at all draw rates. At high draw rates a yield point appears in the stress–strain curves and stress hardening starts immediately following stress drop after yield. At lower strain rates this onset of stress hardening moves to higher strains, indicating the delay of stress-induced crystallization. Competition between orientation and relaxation is the main cause of the latter behaviour. At low strain rates relaxation is dominant, and as a result it takes substantial levels of strains to reach the onset of stress-induced crystallization as compared to the higher stretch rates. This rate dependence of yielding clearly points to the presence of an inherent molecular relaxation mechanism associated with neck formation.

Yield behaviour

The yield stress as a function of temperature is shown in *Figure 7*. This plot shows three distinct linear regions. Yield stress decreases very slowly up to the glass transition temperature. Further increase of temperature causes a rapid decrease of yield stress before reaching a plateau around 147°C. Andrianova *et al.* showed similar behaviour for PET below the glass transition temperature[31]. They attempted to calculate the temperature rise caused by neck formation. However, if there is a temperature rise by neck formation, the drawing stress defined as the minimum stress after yield in the true stress–strain curve should be affected by heat generation at high draw rate, while the yield stress should not. To examine this possibility, the yield stress and the drawing stress as a function of draw rate are compared in *Figure 8*. These results show that the yield stress increases slowly up to a draw rate of 1 mm s^{-1} and then increase abruptly, while the drawing stress increases steadily with the draw rate. This indicates that there is no or very little heat generation. Heat generation causes the mobility of molecules to increase, so that, if this mechanism is dominant, the drawing stress should level off at high draw rates in *Figure 8*. Therefore, it is not appropriate to explain the yield and neck formation of PEN by adiabatic heat generation alone.

Vincent[28] assigned the fall in stress to the effect of decreasing cross-sectional area. Ward[26] emphasized not only the geometrical effect but also the intrinsic load drop in polymers like in metals. From fluctuations shown in true stress–strain curves of PEN, it can be inferred that stress is very localized in certain regions. Therefore, in the case of PEN, yield may occur due to the geometrical effect and the intrinsic load drop, and necking may result from the very localized stress concentration. This behaviour, which as we will demonstrate in the following sections is compounded by a unique molecular mechanism, results in the formation of necks in the films.

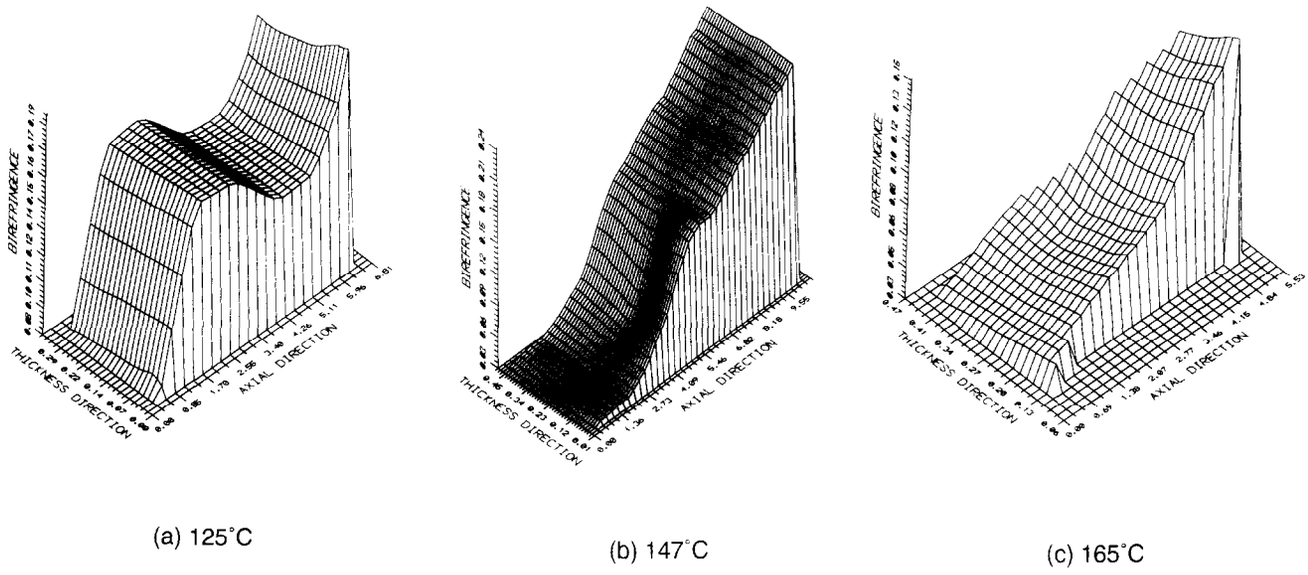

Figure 9 Two-dimensional birefringence distribution along the neck regions of PEN films deformed at (a) 125°C, (b) 147°C and (c) 165°C

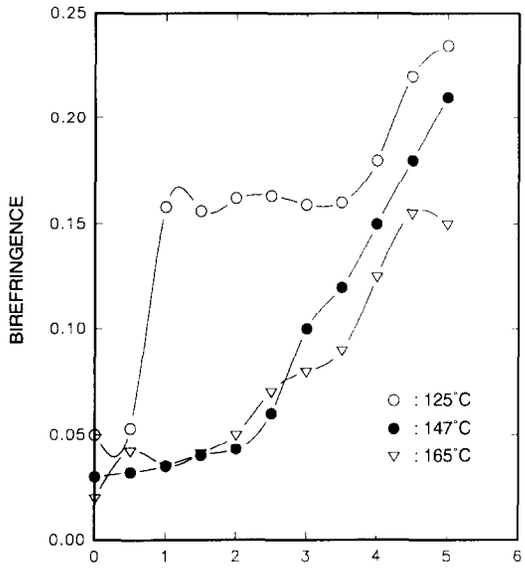

Figure 10 Birefringence Δn_{13} (1 = MD, 3 = ND) as a function of position along the symmetry axis of the MD–ND plane of the neck region.

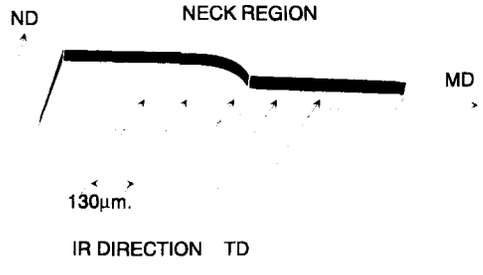

Figure 11 Data sampling positions for i.r. dichroism measurements

Birefringence measurements

In order to investigate the development of optical macro-anisotropy in the neck region, a series of samples were stretched to intermediate stretch ratios where a neck forms and attains a steady drawing but did not disappear. This corresponds to a halfway point between the yield stress and the onset of stress hardening in the stress–strain curves. We have microtomed the samples in the ND–MD plane (3–1) as shown in *Figure 2* and determined the two-dimensional birefringence distribution along the length of the necked regions (*Figure 9*). The birefringence measured in this orientation is one of the out-of-plane birefringences, Δn_{13}. This birefringence is useful in giving highly specific information about the orientation behaviour of the naphthalene groups. The normals of the naphthalene groups exhibit the lowest refractive index and the intrinsic refractive indices along the chain axis are the highest. We have calculated these, assuming additivity of bond polarizabilities[32]. These data are given in *Table 3*. In addition, the difference between the latter two yields the largest intrinsic birefringence values as shown in *Table 3*.

A slice through the mid-thickness in these three-dimensional graphs is shown in *Figure 10* as a function of position along the neck in samples stretched at a series of temperatures above the glass transition temperature. Near T_g the birefringence increases abruptly through the neck region accompanying the rapid reduction in

Table 3 Refractive index and birefringence values of different PEN structures[32]

		All-*trans*-conformations *ttttttt*
Refractive index	n_c	1.908
	n_n	1.360
	n_t	1.808
Birefringence	$\Delta^\circ n_c = n_c - (n_n + n_t)/2$	0.324
	$\Delta^\circ n_{cn} = n_c - n_n$	0.548
	$\Delta^\circ n_{ct} = n_c - n_t$	0.100
	$\Delta^\circ n_{nt} = n_n - n_t$	−0.449

Table 4 Infra-red spectra of PEN[33]

Frequency (cm^{-1})	Assignment[a]	Frequency (cm^{-1})	Assignment
3550	ν(OH)	1400	arom. ring vibr.
3430	Overtone ν(C=O)	1370	$\gamma_w(CH_2)$ *gauche*
3060	ν(arom. CH)	1337	$\gamma_w(CH_2)$ *trans*
3050	ν(arom. CH) crys.	1332	$\gamma_w(CH_2)$ *trans*
2990	$\nu(CH_2)$ crys.	1270	ν(=C–O) + arom.
2965	$\nu(CH_2)$ amorph.	1250	ν(=C–O) + arom.
2910	$\nu(CH_2)$ amorph.	1210	arom. ring vibr.
2890	$\nu(CH_2)$ crys.	1180	naph. ring vibr.
1715	ν(C=O)	1135	naph. ring vibr.
1600	arom. ring vibr.	1090	ν(O–C) *gauche*
1570	arom. ring vibr.	1044	ν(O–C) *gauche*
1500	arom. ring vibr.	930	δ(arom. CH out of plane)
1477	$\delta(CH_2)$ *trans*	835,822,810	$\gamma(CH_2)$, *trans*
1450	$\delta(CH_2)$ *gauche*	765	δ(arom. CH out of plane)

[a] ν = stretching; δ = bending; γ_w = wagging

thickness. As the temperature of stretching is increased, the birefringence profile became more gradual along the neck region.

The birefringence results given above suggest that the planar orientation of naphthalene parallel to the film surface occurs rapidly through the neck region. In order to prove conclusively this rapid alignment hypothesis, *FT*i.r. and micro-beam X-ray diffraction techniques were also used as discussed below.

Infra-red spectra of PEN

I.r. spectra of PET and PEN were compared by Ouchi *et al.*[33]. *Table 4* shows each band in PET and PEN reported by Ouchi *et al.*[33]. In order to obtain positional information along the neck, the i.r. spectra were obtained with the i.r. beam along the TD, as shown in *Figure 11*.

Bands associated with naphthalene ring. Infra-red spectra of PEN5 drawn at 125 and 165°C in the range from 1700 to 450 cm^{-1} are shown in *Figure 12*. I.r.

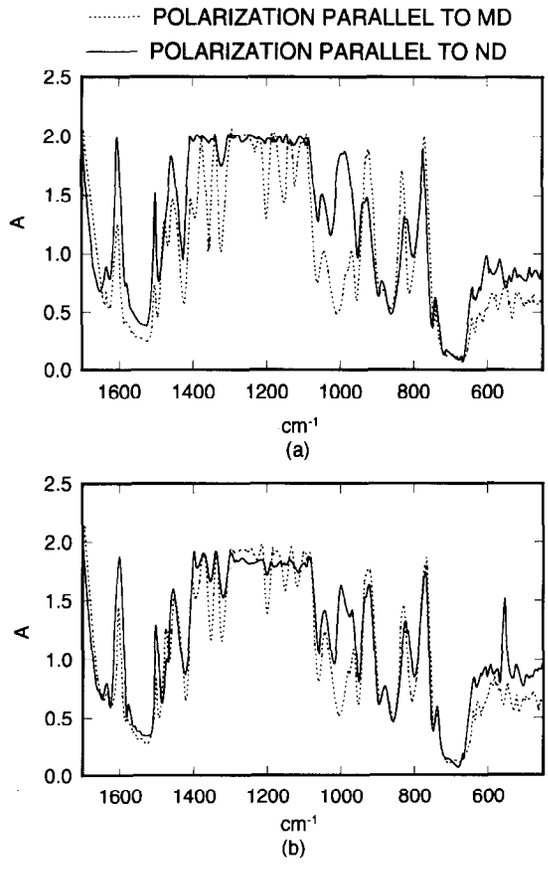

Figure 12 Polarized i.r. spectra on PEN5 films drawn at (a) 125°C and (b) 165°C

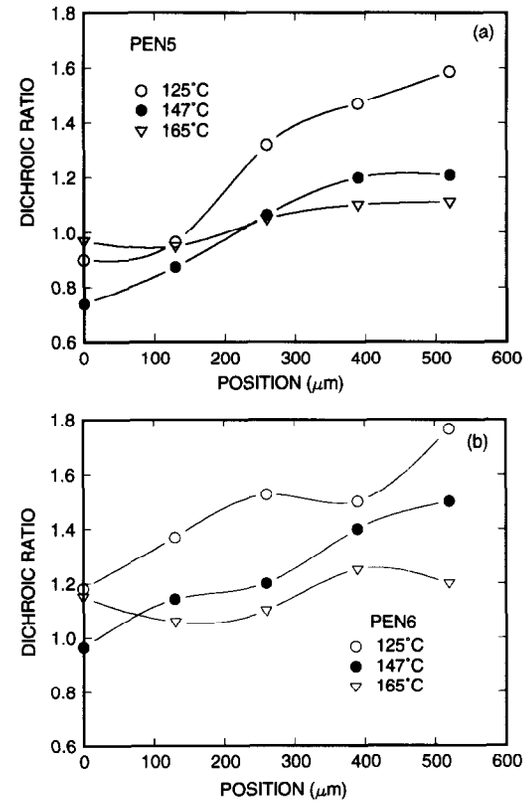

Figure 13 Dichroic ratio of 968 cm^{-1} band vs. position along the neck region of (a) PEN5 and (b) PEN6 films stretched at three processing temperatures

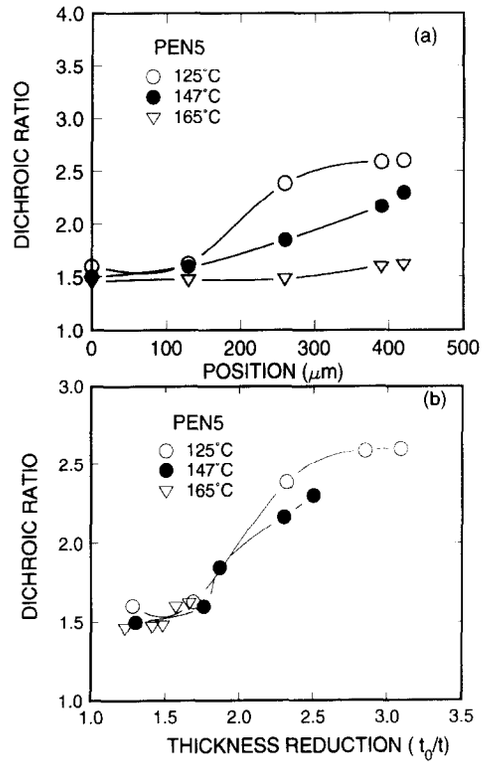

Figure 14 Variation of 1600 cm^{-1} band dichroic ratios of PEN5 (a) as a function of position along the neck and (b) as a function of thickness reduction t_0/t (t_0 = initial thickness and t = local thickness along the neck)

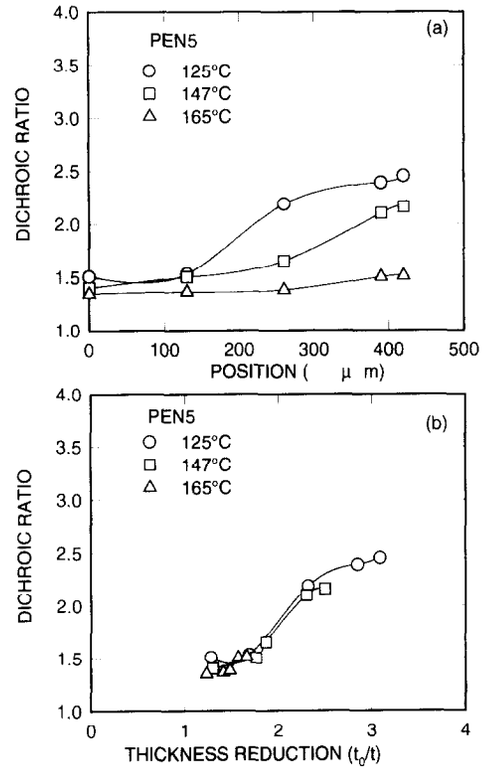

Figure 15 Variation of dichroic ratio for 1500 cm^{-1} band of PEN5 (a) as a function of position along the neck and (b) as a function of thickness reduction along the neck t_0/t (t_0 = initial thickness and t = local thickness along the neck

spectra show too strong absorption in the range from 1400 to 1100 cm^{-1}; as a result we examined the bands at 1600, 1500 and 765 cm^{-1}.

The bands at 1600 and 1500 cm^{-1} were assigned to aromatic ring vibration. The band at 765 cm^{-1} was assigned to aromatic CH out-of-plane vibration[33]. In the case of PET, the 730 cm^{-1} band corresponding to the 765 cm^{-1} band in PEN was a controversial one. According to Miller and Willis[34] the 730 cm^{-1} band was assigned to C–O–C bending vibration. Then, Miyake[35] assigned it to O=C–O out-of-plane bonding vibration. However, Grime and Ward[36] and Liang and Krimm[37] assigned this band to an aromatic CH out-of-plane vibration. Since naphthalene has a strong band at 780 cm^{-1}, Ouchi *et al.* assigned the 765 cm^{-1} band to aromatic CH out-of-plane vibration. This strong out-of-plane CH bending vibration is more useful than in-plane bands. This band results from strong coupling with adjacent hydrogen atoms and can be used to assign the position of substituents on the aromatic ring.

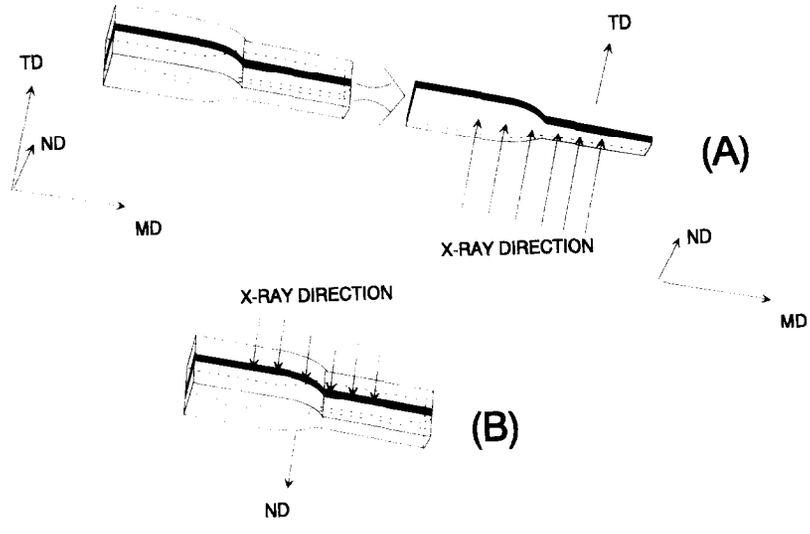

Figure 16 Micro-beam X-ray WAXS patterns taken along the neck region (A) with the X-ray beam in the TD and (B) with the X-ray beam along the normal direction

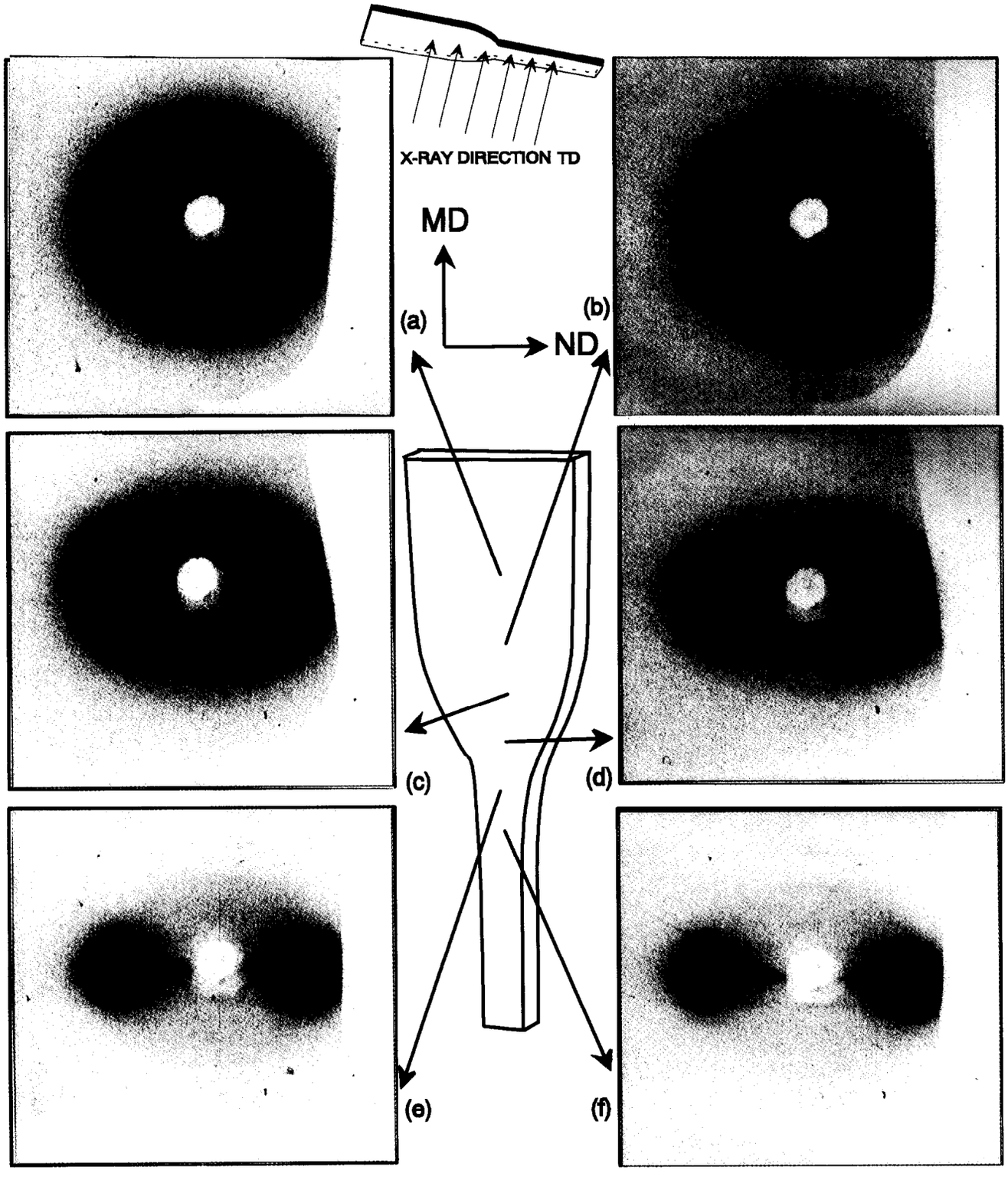

Figure 17 Micro-beam WAXS patterns of PEN5 neck region on the ND–TD microtomed slice with the X-ray direction parallel to the transverse direction. Processing temperature 103°C. Positions (a) 0, (b) 130, (c) 260, (d) 390, (e) 520 and (f) 650 μm. (Neck shape shown above is proportionally drawn)

Bands associated with gauche *and* trans *conformation.* The 822 cm^{-1} band (*gauche*) assigned to CH_2 rocking vibration shows sharp s polarization, so that this band disappears when the polarization is parallel to the machine direction. A band appears at 810 cm^{-1} when the polarization is perpendicular to the machine direction, indicating p polarization as shown in *Figure 12*, which is consistent with Ouchi's results. He observed that crystallization or drawing resulted in new bands at 810 and 835 cm^{-1}. In our study, the 835 cm^{-1} band does not appear by drawing.

Dichroic ratios of 968 and 822 cm^{-1} bands. Dichroic ratios of the *trans* and *gauche* rotational isomers of the ethylene glycol moiety in the repeat unit as a function of position along the neck have been determined. The

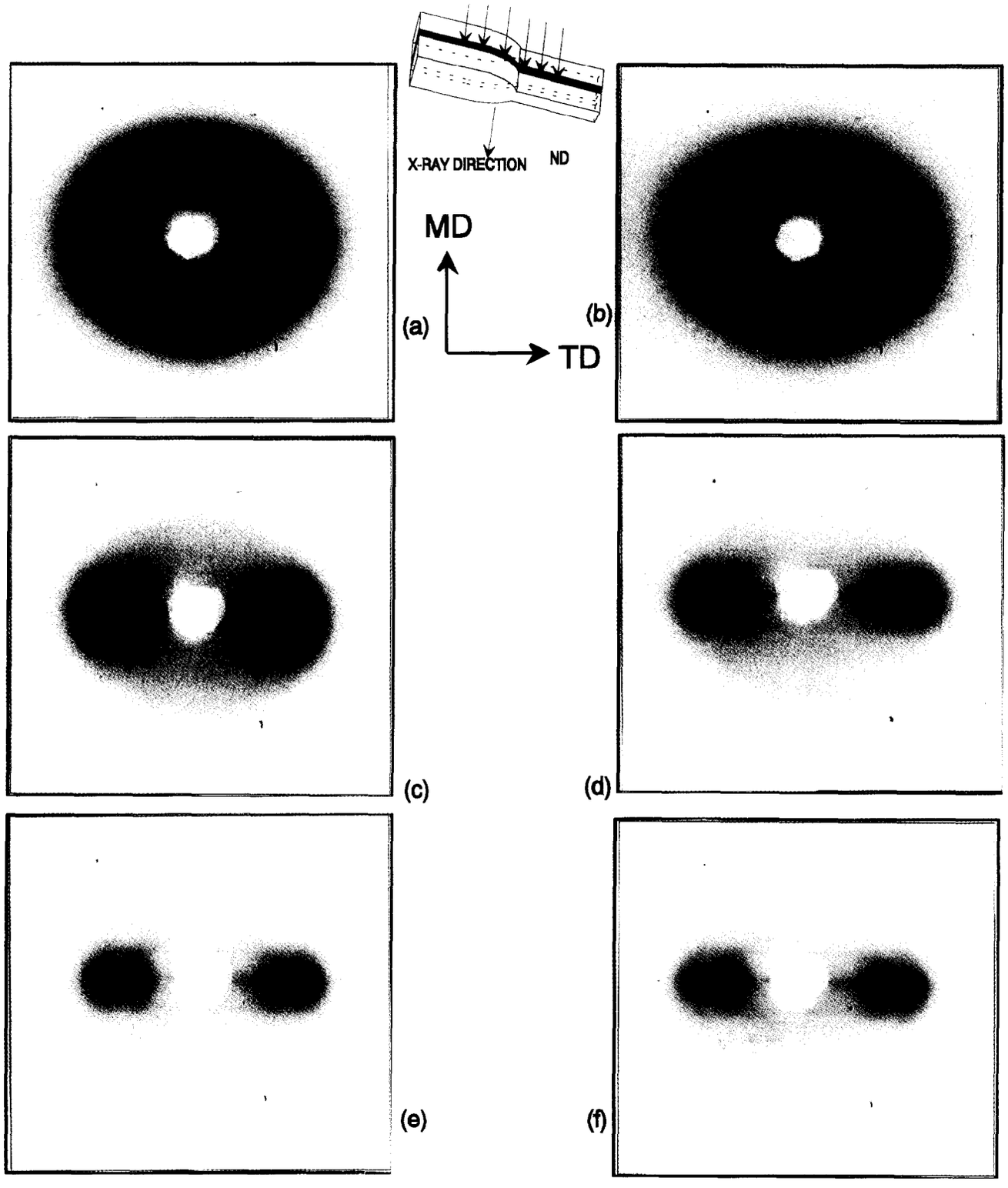

Figure 18 Micro-beam WAXS patterns of PEN5 neck region with the X-ray direction parallel to the normal direction. Processing temperature 103°C. Positions (a) 0, (b) 130, (c) 260, (d) 390, (e) 520 and (f) 650 μm

importance of these data relates to the fact that only the *trans* rotational isomer exists in the crystalline state, and so the proportion and degree of orientation of this isomer will greatly influence the deformation behaviour of PEN film. However, the thickness-independent band has not been verified in the case of PEN, so that only the dichroic ratios of the *trans* and *gauche* rotational isomers have been determined.

The absorption band at 968 cm^{-1} was assigned to the *trans* conformational state. The dichroic ratio increases along the neck, as shown in *Figure 13*. This is consistent with the birefringence results shown in the previous section.

Dichroic ratios of 1600 and 1500 cm^{-1} bands. In order to investigate the orientation behaviour of naphthalene

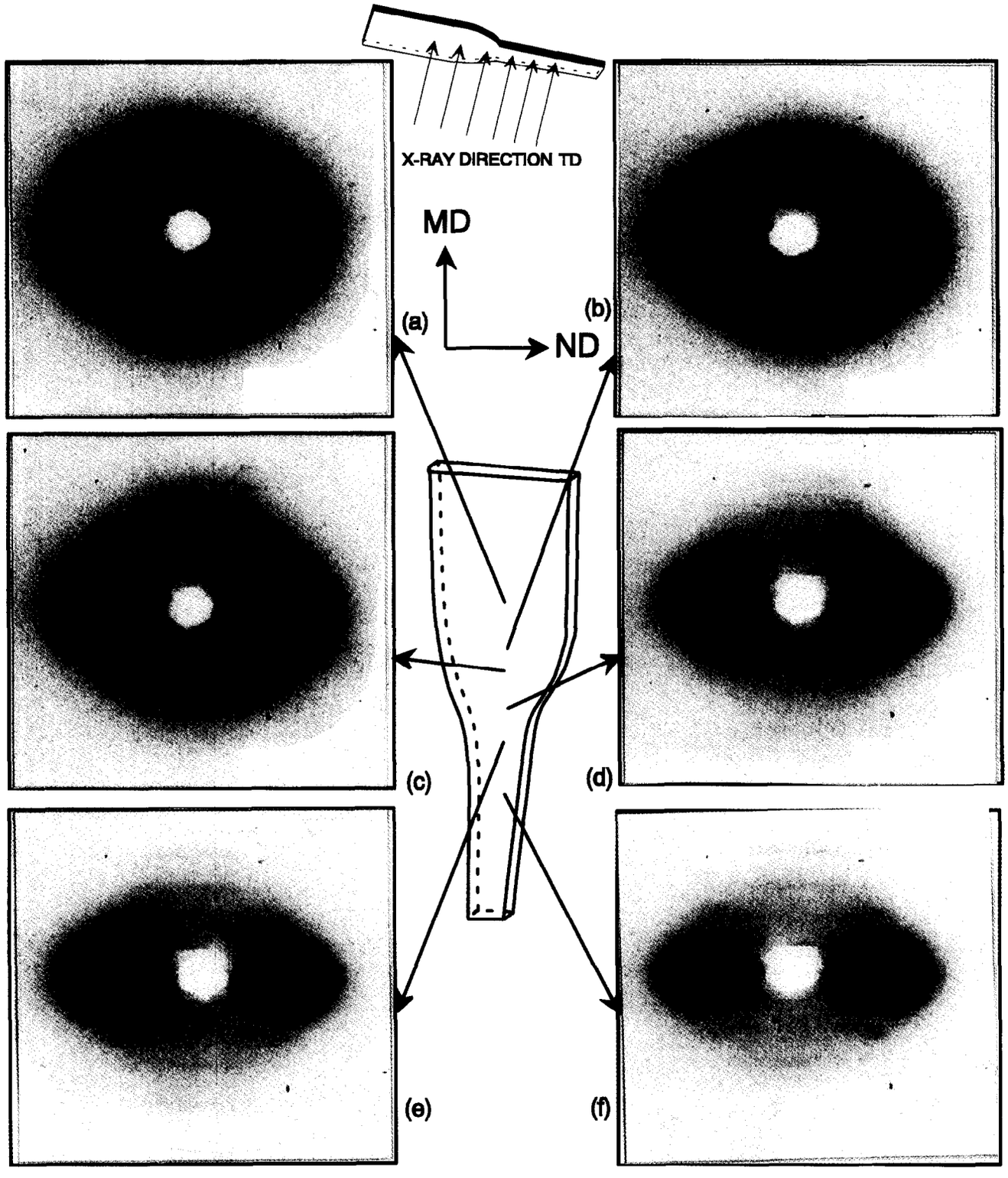

Figure 19 Micro-beam WAXS patterns of PEN5 neck region on an ND–TD microtomed slice with the X-ray direction parallel to the transverse direction. Processing temperature 125°C. Positions (a) 0, (b) 130, (c) 260, (d) 390, (e) 520 and (f) 650 μm. (Neck shape shown above is proportionally drawn)

planes, the 1600 and 1500 cm^{-1} bands associated with this chemical group were examined and are shown in *Figures 14* and *15* respectively.

Figures 14a and *15a* show the dichroic ratio as a function of position along the neck for samples stretched at three different temperatures. Before the neck region (position less than 100 μm), the dichroic ratio is constant. In the neck, this dichroic ratio increases abruptly and levels off at its highest value after the neck. This indicates the alignment of naphthalene planes parallel to the surface of the samples. When the local dichroic ratios are plotted against local thickness reduction ($= t_0/t$) (*Figures 14b* and *15b*), the data collapse onto a single curve. This temperature insensitivity of the dichroic ratio vs. deformation suggests that there is a direct link between the thickness strain and the

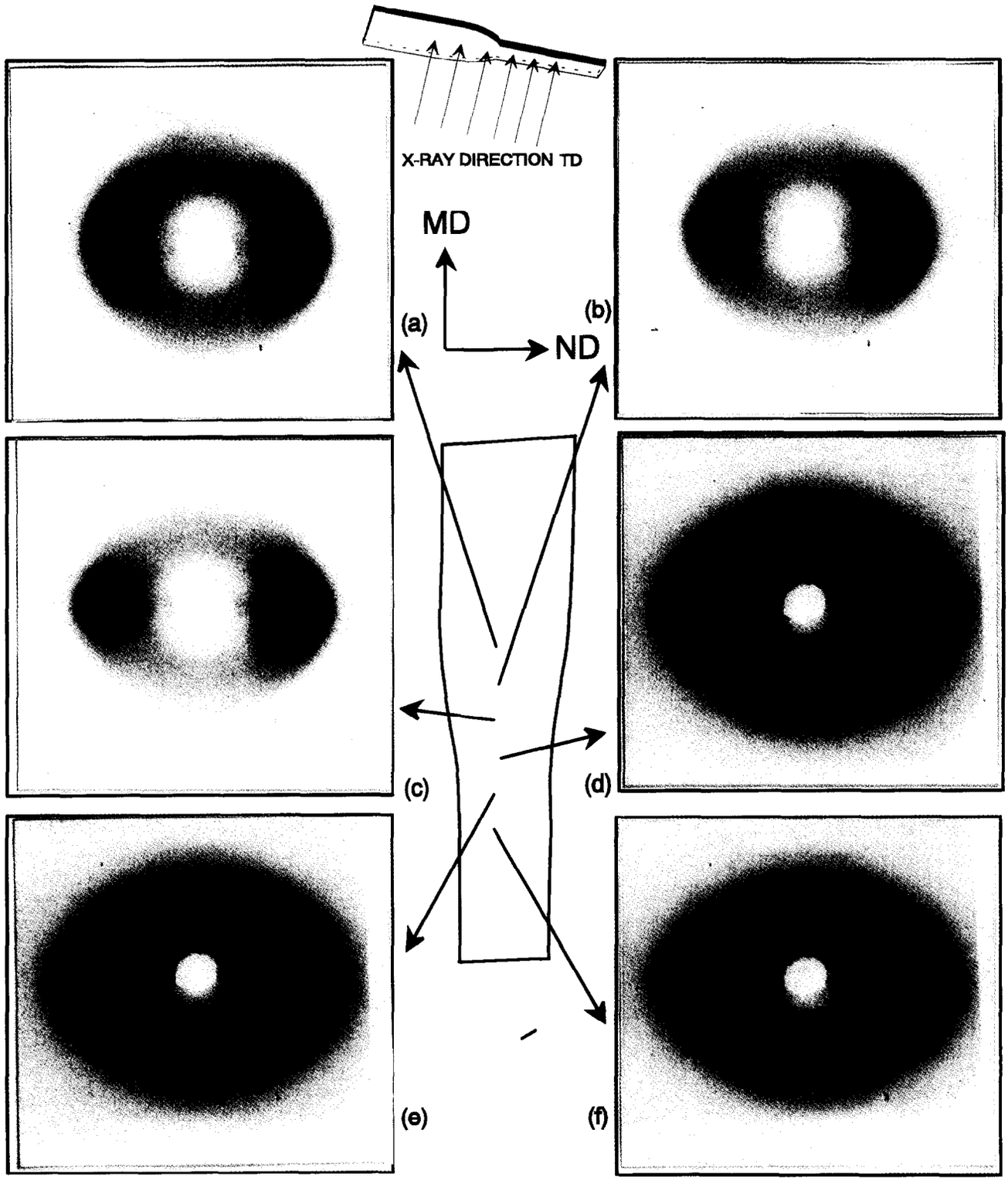

Figure 20 Micro-beam WAXS patterns of PEN5 neck region on an ND–TD microtomed slice with the X-ray direction parallel to the transverse direction. Processing temperature 147°C. Positions (a) 0, (b) 130, (c) 260, (d) 390, (e) 520 and (f) 650 μm. (Neck shape shown above is proportionally drawn)

cooperative alignment of the naphthalene planes and thus neck formation.

Micro-beam wide-angle diffraction studies along the neck

In order to study the development of crystalline orientation along the neck region, we used a matrixing micro-beam X-ray diffraction camera developed in our group. In this camera a series of WAXS patterns can be obtained at 100 μm intervals (diameter of the X-ray beam) using a precision XY stage without dismounting the samples, thereby preserving the spatial registry between consecutive WAXS patterns. X-ray WAXS patterns were taken at a series of locations with the X-ray beam directed along TD (*Figure 16a*) and ND directions (*Figure 16b*).

Figure 17 shows such WAXS patterns of PEN5 drawn

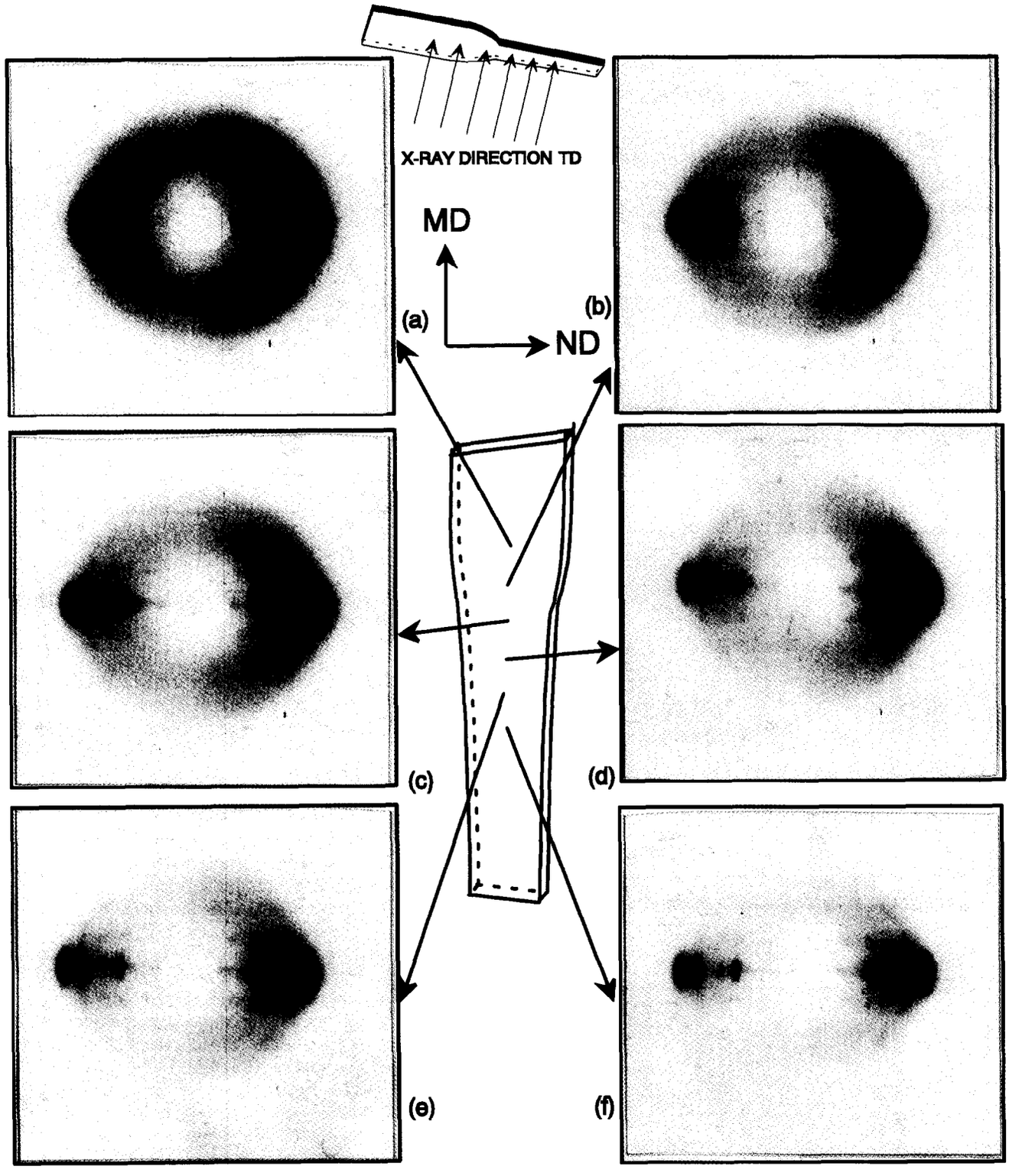

Figure 21 Micro-beam WAXS patterns of PEN5 neck region on the ND–TD microtomed slice with the X-ray direction parallel to the transverse direction. Processing temperature 165°C. Positions (a) 0, (b) 130, (c) 260, (d) 390, (e) 520 and (f) 650 μm. (Neck shape shown above is proportionally drawn)

at 103°C. The patterns shown in this figure are taken with the X-ray beam along the transverse direction at the positions indicated on the proportionally sketched (ND–MD) neck profile. Before the neck region, a typical isotropic broad amorphous halo is observed (*Figures 17a* and *17b*). As the beam probes further into the neck region, the intensity begins to concentrate along the transverse direction (*Figures 17c–e*) as a result of orientation. In addition, this concentration of intensity also takes place in the 2θ direction towards the higher-angle side of the distribution where the (1 0 0) and ($\bar{1}$ 1 0) planes are expected to develop with increasing crystal perfection. Since naphthalene ring planes make an angle of about 4.7° with the ($\bar{1}$ 1 0) plane, it can be easily inferred that naphthalene ring planes become oriented parallel to the film surface along the neck

region. This is confirmed in *Figure 18* where WAXS patterns of the same sample were taken along the normal direction. In these patterns, the main feature is the presence of the (0 1 0) plane, which was totally absent in *Figure 17*, confirming the presence of uniplanar axial texture development along the neck region. It should be noted that the absence of reflections in layer lines above the equator in *Figures 17* and *18* indicates poor interchain registry along the chain axes. In other words, three-dimensional order is absent and local structural order resembles nematic order with the ordering direction (director!) coincident with the normals of the naphthalene planes. This is also evident in *Figure 17* where layer lines appear as streaks typical of such disorder.

Wide-angle X-ray diffraction patterns of PEN5 drawn at 125°C are shown in *Figure 19*. Before the neck, diffraction intensity is stronger than for PEN5 drawn at 103°C and it shows intensity concentrations in the normal direction. This indicates that, prior to the development of a neck, PEN deforms further at 125°C compared to 103°C as a result of higher chain mobility. As the thickness strain is increased, the change of diffraction pattern with strain is similar to those obtained in *Figure 19*. However, in these cases (0 1 0) planes are observed in the WAXS patterns in addition to the precursors of (1 0 0) and ($\bar{1}$ 1 0) (*Figures 19d–f*). The ($\bar{1}$ 1 0) reflection also shows extremely small azimuthal spread, indicating very high orientation of naphthalene ring planes parallel to the film surface.

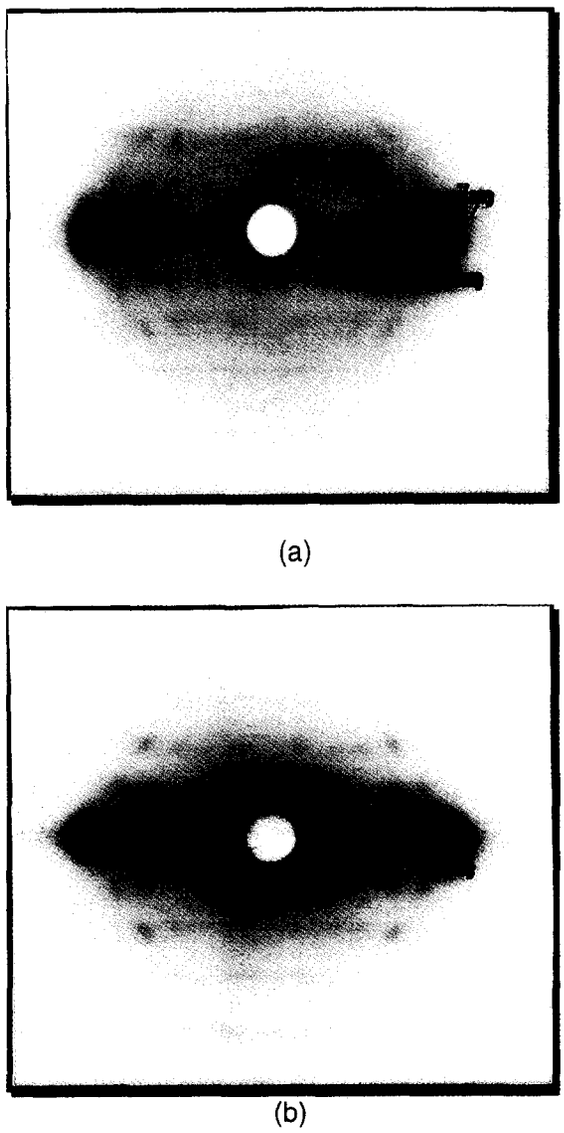

Figure 22 (a) Enlargement of WAXS pattern shown in *Figure 21* identifying the prominent α and β peaks. (b) WAXS pattern of high-speed-spun PEN fibre showing only the α peaks[38]

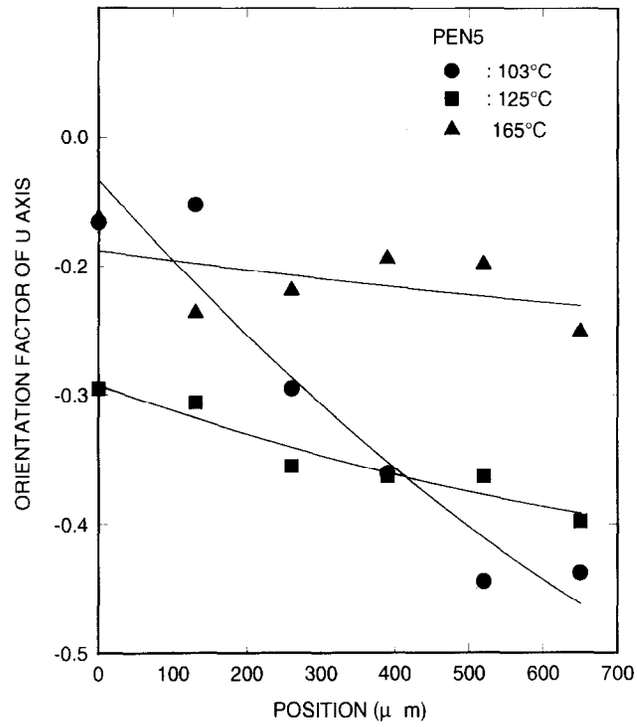

Figure 23 Variation of orientation factor of normals of naphthalene planes along the neck region

Figure 20 represents WAXS film patterns of PEN5 drawn at 147°C. Before the neck shown in *Figure 20a* the general character of the WAXS pattern is similar to those seen in *Figures 18* and *19*, except that at this temperature we observe even higher orientation of amorphous regions in the unnecked regions (*Figures 20a* and *20b*). Crystalline reflections begin to appear early in the neck region, (0 1 0) as well as precursors of (1 0 0) and ($\bar{1}$ 1 0). From *Figure 20* one can observe the increase of intensity of the ($\bar{1}$ 1 0) reflection, and even in the neck region ($\bar{1}$ 1 0) shows a sharp arc on the equator. One can also distinguish (1 0 0) and ($\bar{1}$ 1 0) reflections from *Figure 20*. These results suggest that transverse isotropy is present in these samples, resulting in a random distribution of ($\bar{1}$ 1 0) planes in the transverse direction. At this temperature, three-dimensional order is still absent in the neck region as indicated by the absence of higher-order peaks.

At 165°C, the deformation no longer becomes highly localized. Instead it occurs in a wider range. This is also reflected in the WAXS patterns in *Figure 21*, where the first signs of three-dimensional order begin to emerge particularly in the regions where higher deformation has taken place (*Figures 21d–f*). Furthermore, at this temperature, additional peaks appear in the WAXS patterns as demonstrated in *Figure 22a* where

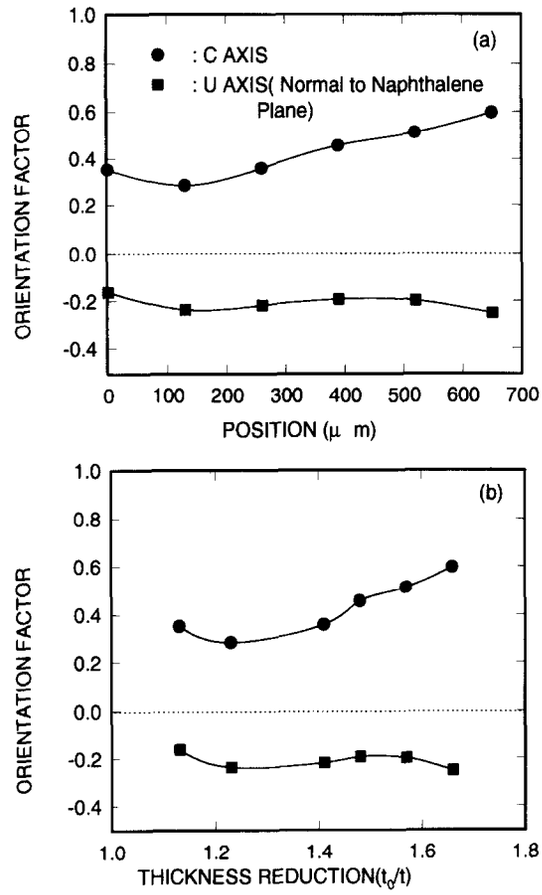

Figure 24 Orientation factors of U axis (normal to the naphthalene plane) and the c-axis (a) as a function of position along the neck and (b) as a function of thickness reduction t_0/t (t_0 = initial thickness)

an enlarged WAXS pattern is shown together with a WAXS pattern of high-speed-spun PEN fibre showing only the α-phase peaks[38]. In this pattern (*Figure 22a*), in addition to α-phase peaks, a β-phase ($\bar{2}$ 2 0) peak in the equator and ($\bar{1}$ 1 1) peak in the first layer line are observed. In addition, we obtained WAXS patterns with the X-ray beam directed along the normal direction at a series of locations (not presented in this paper) and found that they are very similar to those obtained with the beam in TD (*Figure 21*). This also confirmed that, at very high deformation temperatures, the texture changes to transverse isotropy.

Orientation factors of naphthalene ring planes

In order to quantify the orientation of the c axes and the normals of the naphthalene planes, values of $\langle\cos^2\chi_{U,Z}\rangle$ and $\langle\cos^2\chi_{100,Z}\rangle$ were determined from the azimuthal intensity distributions of drawn PEN shown in the previous section. The orientation factor of the naphthalene ring plane was determined as:

$$f = (3\langle\cos^2\chi_{U,Z}\rangle - 1)/2$$

As shown in *Figure 23*, the sample deformed at lower temperature shows the steepest change in the naphthalene plane normal orientation. Here $f = -0.5$ indicates perfect alignment of the naphthalene planes parallel to the film surface. As the deformation temperature increases, this sharp orientational gradient along the neck region decreases.

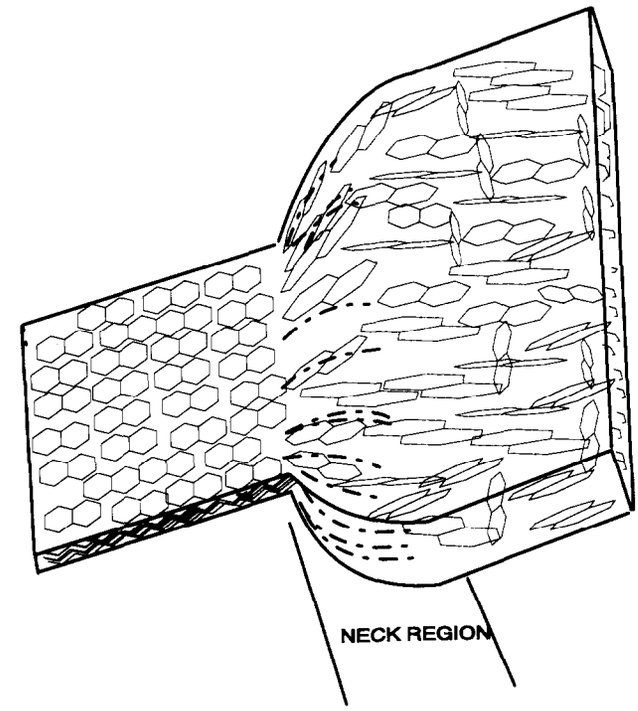

Figure 25 Structural model for the naphthalene ring orientation along the neck region

However, the orientation factor of the chain axis could not be determined except for PEN drawn at 165°C owing to the strong overlap of amorphous and crystalline diffraction peaks. The orientation factors of U axis (normal to the naphthalene ring plane) and c axis (chain axis) are shown in *Figure 24*. The chain axis orientation factor for PEN drawn at 165°C is not so high owing to the higher chain mobility at this temperature.

CONCLUSIONS

In this paper, highly localized cooperative orientation of flat naphthalene groups parallel to the surface of films is identified as the molecular mechanism responsible for the formation of a neck in uniaxially stretched amorphous PEN films. This mechanism persists at deformation temperatures as high as 20–30°C above the glass transition temperature. This unusual highly localized cooperative reorientation occurs in a manner resembling an isotropic–nematic transition and macroscopically appears as a neck. This mechanism was verified at several different structural levels by birefringence, i.r. dichroism and micro-beam WAXS techniques.

From these observations, the model of naphthalene ring plane alignment along the neck is proposed as in *Figure 25*. Before, the neck the naphthalene planes are randomly oriented. After the neck, these planes are rapidly aligned, exhibiting one-dimensional nematic-like order in the thickness direction.

As a result of this preferential orientation of the naphthalene planes parallel to the broad surface of the films upon deformation, the samples were found to exhibit uniplanar axial ($\bar{4}$ 3 0)[0 0 1] texture in the temperature range $T_g \pm 20$°C. The ($\bar{4}$ 3 0) planes are roughly parallel to the naphthalene planes in the polymer chain. At higher temperatures the sample texture was found to approach transverse isotropy,

which is the usually expected texture in unconstrained uniaxial stretching.

ACKNOWLEDGEMENTS

We wish to thank Dr William Boone of Goodyear Tire and Rubber Co. for providing the cast sheets of poly(ethylene naphthalate). Financial support for this research was provided partially by National Science Foundation, Presidential Young Investigator Program DDM-8858303 (M. Cakmak).

REFERENCES

1 Cook, J. G., Huggill, H. P. W. and Lowe, A. R. Br. Pat. 604073, 1946
2 Mencik, Z. *Chem. Prim.* 1967, **17**, 78
3 Cakmak, M., Wang, Y. D. and Simhambhatla, M. *Polym. Eng. Sci.* 1990, **30** (2), 721
4 Desai, A. B. and Wilkes, G. L. *J. Polym. Sci. Symp.* 1974, **46**, 291
5 Makarewicz, P. J. and Wilkes, G. L. *J. Appl. Polym. Sci.* 1978, **22**, 3347
6 Ouchi, I., Aoki, H., Shimotsuma, S., Asai, T. and Hosoi, M. Proc. 17th Japan Congr. Materials Research, 1974, p. 217
7 Fukurawa, T. and Sakai, K. *Japan Plast. Age* June 1974, p. 20
8 Buchner, S., Wiswe, D. and Zachmann, H. G. *Polymer* 1989, **30**, 480
9 Cheng, S. Z. D. and Wunderlich, B. *Macromolecules* 1989, **21**, 789
10 Ghanem, A. M. and Porter, R. S. *J. Polym. Sci. (B) Polym. Phys.* 1989, **27**, 2587
11 Cheng, S. Z. D., Janimak, J. J., Zhang, A., Guan, J. and Chu, A. L. *Polym. Bull.* 1988, **20**, 449
12 Hayashi, S., Ishiharada, M. and Saito, S. *Polym. J.* 1985, **17** (8), 953
13 Fisher, E. W. and Schmidt, G. F. *Angew. Chem.* 1962, **74**, 551
14 Peterlin, A. *J. Polym. Sci. (C)* 1965, **9**, 61; 1967, **15**, 427; 1969, **18**, 123
15 Hay, I. L. and Keller, A. *Kolloid Z. Z. Polym.* 1965, **204**, 43
16 Stein, R. S. *Proc. R. A. Welch Found. Conf. Chem. Res.* 1967, **10** (Polym.), 207
17 Bonart, R. *Kolloid Z. Z. Polym.* 1966, **211**, 14
18 Peterlin, A. 'Man Made Fibers', Vol. 1 (Eds H. F. Mark, S. M. Atlas and E. Cernia), Wiley Interscience, New York, 1967, pp. 283–340
19 Peterlin, A. *Kolloid Z. Z. Polym.* 1967, **216/217**, 129
20 Peterlin, A. *Polym. Eng. Sci.* 1969, **9**, 172
21 Fisher, E. W. and Goddar, M. *J. Polym. Sci. (C)* 1969, **16**, 4405
22 Stein, R. S. *Polym. Eng. Sci.* 1969, **9**, 320
23 Peterlin, A. *J. Mater. Sci.* 1969, **6**, 490
24 Kasai, N. and Kakudo, M. *J. Polym. Sci. (A)* 1964, **2**, 1955
25 Marshall, I. and Thompson, A. B. *Proc. R. Soc. (A)* 1954, **221**, 541
26 Ward, I. M. 'Mechanical Properties of Polymers', Wiley Interscience, New York, 1985
27 Lazurkin, Y. S. *J. Polym. Sci.* 1958, **30**, 395
28 Vincent, P. *Polymer* 1960, **1**, 7
29 Alexander, L. E. 'X-Ray Diffraction Methods in Polymer Science', Wiley, New York, 1969
30 Wilchinsky, Z. W. *J. Appl. Phys.* 1959, **30**, 792
31 Andrianova, G. P., Arutyunov, B. A. and Popov, Y. U. *J. Polym. Sci., Phys.* 1978, **16**, 1139
32 Ozisik, R., Venkatesvaran, H., Cakmak, M., Bahar, I. and Erman, B. *Polymer* in prep.
33 Ouchi, I., Hosoi, M. and Shimotsuma, S. *J. Appl. Polym. Sci.* 1977, **21**, 3445
34 Miller, R. G. J. and Willis, H. A. *J. Polym. Sci.* 1956, **19**, 485
35 Miyake, A. *J. Polym. Sci.* 1959, **38**, 479, 496
36 Grime, D. and Ward, I. M. *Trans Faraday Soc.* 1958, **54**, 959
37 Liang, C. Y. and Krimm, S. *J. Mol. Spectrosc.* 1959, **3**, 554
38 Kim, J. C. and Cakmak, M. *J. Appl. Polym. Sci.* to be submitted